Journal of Building Engineering 95 (2024) 110171

Contents lists available at ScienceDirect

Journal of Building Engineering

journal homepage: www.elsevier.com/locate/jobe

Modeling time-dependent deformation in concrete: A fractional calculus method with finite element implementation

Xianming Luo [a], Yun Zhou [b,*], Fan Yi [a], Weijian Yi [a]

[a] College of Civil Engineering, Hunan University, Changsha, 410082, China
[b] Key Laboratory for Damage Diagnosis of Engineering Structures of Hunan Province, Key Laboratory of Building Safety and Energy Efficiency of the Ministry of Education, College of Civil Engineering, Hunan University, Changsha, 410082, China

ARTICLE INFO

Keywords:
Fractional calculus
Time-dependent deformation
Concrete material modeling
Finite element analysis

ABSTRACT

This study presents a novel numerical method to simulate the time-dependent behavior of concrete materials. The deformation response of both traditional and fractional calculus (FC) viscoelastic models is analyzed by the proposed method, in which models' one-dimensional constitutive relationships are extended to the three-dimensional form. By applying numerical and finite difference methods based on Caputo-type fractional integration, the stress-strain behavior of the FC viscoelastic model is discretized over the time scale. This method exhibits broad application prospects, and can be employed to represent various forms of viscoelastic models. For the concrete material, suitable FC viscoelastic models are developed. To facilitate practical engineering applications of the proposed model, a numerical solution algorithm is implemented in the finite element (FE) analysis through the User-defined Material Mechanical Behavior (UMAT) interface of the commercial FE software ABAQUS. Finally, FE results are compared with the experimental results from several concrete creep tests. The consistency between the FE results and experimental data confirms the effectiveness of the proposed model in describing concrete behavior. The proposed method and model provide theoretical and numerical support for a more profound understanding and simulation of the time-dependent deformation of RC specimens in practical engineering applications.

1. Introduction

As a commonly used construction material, concrete has obtained widespread application in various infrastructure and building projects due to its superior strength and durability. However, under prolonged loading conditions, concrete exhibits a gradually evolving deformation behavior known as creep. A profound understanding of the creep characteristics of concrete is the crux for the design and maintenance of structures, e.g., dams [1], high-rise buildings [2,3], and prestressed structures [4,5], in which the influence of concrete's time-dependent behavior cannot be ignored. Concrete is a complex and compound material, of which creep behavior is influenced by various factors, including concrete strength, type of cement, loading history, temperature variations, and even the composition of concrete constituents.

Previous studies on concrete creep behavior primarily relied on laboratory tests conducted on standard specimens. In these experiments, researchers typically applied varying levels of load and monitored the strain process of the specimens to investigate concrete creep performance under different parameters and conditions. Even so, researchers typically resort to empirical formulas

* Corresponding author.
E-mail addresses: luoxianming@hnu.edu.cn (X. Luo), zhouyun05@hnu.edu.cn (Y. Zhou), yifance@hnu.edu.cn (F. Yi), wjyi@hnu.edu.cn (W. Yi).

https://doi.org/10.1016/j.jobe.2024.110171
Received 30 May 2024; Received in revised form 25 June 2024; Accepted 6 July 2024
Available online 16 July 2024

obtained from regression analysis committing results of general applicability from these experimental data. This approach aims to identify the correlations inherent in experimental data and establish theoretical models describing the deformation trends of concrete over time. For instance, organizations such as the American Concrete Institute (ACI 209 R [6]) and Ceb-*fip* (MC2010 [7]) have suggested empirical formulas for concrete creep calculation formulation. Subsequently, Bazant et al. [8–12] have proposed several semi-empirical predictive models for the time-dependent deformation of concrete, based on the theory of micro-prestressing solidification and a database recorded by RILEM with substantial experiments of concrete shrinkage and creep. However, these models involve complex computational forms and numerous parameters, some of which are challenging to obtain during the structural design phase. In 2000, Gardner and Lockman [13] introduced a more concise yet reasonably accurate model. The model can be used regardless of what chemical admixtures or mineral by-products are in the concrete, the casting temperature, or the curing regime. The primary focus of the aforementioned works is to develop a computational formula for determining the strain-time relationship in concrete under certain loading conditions. The formula is yet limited since it is only applicable when the stress in concrete is below 0.4 f_c, which is a threshold that concrete obeys a linear relationship between stress and strain. The previous work, more unfortunately, did not establish a coherent physical model for the deformation constitutive behavior of concrete. Moreover, the current concrete shrinkage and creep formulas are only applicable to a limited range of specific concrete types, such as ordinary and high-strength concrete. For other new types of concrete [14,15], these formulas are no longer applicable, and a whole new set of formulas needs to be derived to perform the corresponding calculations.

By its definitions, viscoelastic materials simultaneously exhibit both viscous and elastic characteristics during the deformation process. The time-dependent deformation and flow characteristics of materials under loading are commonly simulated by viscoelastic material models, which consist of a series of elements (springs or dashpots) arranged in series or parallel, such as Maxwell, Kelvin-Voigt, and Zener, etc. Carol et al. [16] proposed a constitutive model applicable to concrete based on the viscoelastic material model. Santhikumar et al. [17] established a constitutive analytical model for a Kelvin-Voigt chain viscoelastic model, which is used to analyze the tensile softening phenomenon over time in aging materials like concrete. Han et al. [18] proposed a viscoelastic-plastic model consisting of six elements to simulate the creep behavior of concrete, revealing the nonlinear characteristics of concrete under high-stress conditions. Luzio [19] presented a finite-element formulation for the analysis of time-dependent failure of concrete using a Maxwell chain model. Honorio et al. [20] delved into the aging, relaxation, and creep mechanisms of concrete-type materials through modeling and analyzing the multiscale aging viscoelastic properties of different internal components**.** Aiming for an accurate depiction of material characteristics, viscoelastic models typically involve a series of basic elements arranged in a chain architecture, which demand numerous input parameters and have a complex analytical form, making them less favorable for calculations [21]. Additionally, the response of conventional viscoelastic models is controlled by ordinary differential equations, so they mathematically follow exponential laws. However, some scholars have found that the creep characteristics of materials follow power laws rather than exponential laws [22]. Therefore, a material model based on fractional calculus (FC) was proposed and has been widely applied to various engineering materials [23–28], i.e., replacing the integer order derivatives of stress or strain with fractional orders in the expressions of traditional viscoelastic models. This is called the FC viscoelastic model, which has demonstrated obvious advantages on reducing the number of required parameters when fitting experimental data.

Currently, the FC model is primarily applied to fit experimental results reducing the number of parameters in the fitting process [29]. However, the mechanical properties of the FC model are limitedly studied. In analytical approaches, researchers utilize integral transformations to determine the response of the FC mechanical model [30,31], but obtaining analytical solutions is inaccessible when the model is complex. Furthermore, theoretical models are typically one-dimensional, restricting their practical applicability. Despite the FC model being proposed early [32], its numerical methods or FE implementations have primarily focused on one-dimensional models [33–35] while the three-dimensional case is rarely studied. The status quo is owing to the fact that considerations of three-dimensional constitutive behavior involving material Poisson's ratio and multi-axial constitutive relations, and only a handful of studies have been conducted on several specific materials models, such as FMM (Fractional Maxwell Model) [36], FZM (Fractional Zener Model) [37,38], and FSLS(Fractional Standard-linear-solid Model) model [39,40]. For other typical fractional viscoelastic models, there is still a lack of detailed implementation methods in commercial FE software [38]. Moreover, the discretization of the constitutive relations over time scales is required in the FE implementation, which faces certain challenges due to the diverse forms of numerical solutions and the different definitions of fractional calculus. To incorporate FC models effectively in representing the behavior of materials, it is essential to implement these constitutive models into FE software using a general approach. Substantial efforts have been dedicated to the theoretical aspects of 1D fractional constitutive laws [35], along with addressing experimental considerations and parameter characterization [25,40–42]. Most existing studies employ expressions involving the Mittag-Leffler function to represent creep/relaxation compliance [39,40] and characterize the stress-strain constitutive relationship. However, this type of constitutive relationship requires repeated calculations of the Mittag-Leffler function in each time increment that computational efficiency is significantly reduced. Therefore, more efficient and accurate numerical computation methods are desired to facilitate the application of any FC model in FE analyses.

This study develops a computational expression and three-dimensional constitutive relations applicable to various FC models. Based on the characteristics of concrete and employing numerical methods with Caputo-type fractional calculus, the present work proposed a novel FC-based viscoelastic model and a numerical computation method suitable for concrete materials. The proposed models are implemented using Fortran and the interface of commercial FE software (ABAQUS, UMAT), in which validation is also performed utilizing experimental results from several concrete creep tests.

Table 1
Traditional and FC viscoelastic model.

	Model diagram	Constitutive equation	P & Q	
Maxwell Model	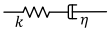	$\sigma(t)+\frac{\eta}{k}\frac{\mathrm{d}\sigma(t)}{\mathrm{d}t}=\eta\frac{\mathrm{d}\varepsilon(t)}{\mathrm{d}t}$	$P=1+\frac{\eta}{k}\frac{\partial}{\partial t}$	$Q=\eta\frac{\partial}{\partial t}$
Kelvin-Voigt Model	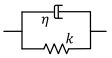	$\sigma(t)=k\varepsilon(t)+\eta\frac{\mathrm{d}\varepsilon(t)}{\mathrm{d}t}$	$P=1$	$Q=k+\eta\frac{\partial}{\partial t}$
SLS Model (Zener model)	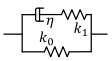	$\sigma(t)+\frac{\eta}{k_1}\frac{d\sigma(t)}{dt}=k_0\varepsilon(t)+\frac{\eta(k_0+k_1)}{k_1}\frac{d\varepsilon(t)}{dt}$	$P=1+\frac{\eta}{k_1}\frac{\partial}{\partial t}$	$Q=k_0+\frac{\eta(k_0+k_1)}{k_1}\frac{\partial}{\partial t}$
Single Fractional Model	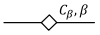	$\sigma(t)=C_\beta\frac{\mathrm{d}^\beta\varepsilon(t)}{\mathrm{d}t^\beta}$	$P_f=1$	$Q_f=C_\beta\frac{\partial^\beta}{\partial t^\beta}$
Fractional-KV Model		$\sigma(t)=C_\alpha\frac{\mathrm{d}^\alpha\varepsilon(t)}{\mathrm{d}t^\alpha}+C_\beta\frac{\mathrm{d}^\beta\varepsilon(t)}{\mathrm{d}t^\beta}$	$P_f=1$	$Q_f=C_\alpha\frac{\partial^\alpha}{\partial t^\alpha}+C_\beta\frac{\partial^\beta}{\partial t^\beta}$
Fractional-Zener Model	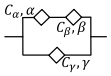	$\sigma(t)+\frac{C_\alpha}{C_\beta}\frac{\mathrm{d}^{\alpha-\beta}\sigma(t)}{\mathrm{d}t^{\alpha-\beta}}=C_\alpha\frac{\mathrm{d}^\alpha\varepsilon(t)}{\mathrm{d}t^\alpha}+C_\gamma\frac{\mathrm{d}^\gamma\varepsilon(t)}{\mathrm{d}t^\gamma}+\frac{C_\alpha C_\gamma}{C_\beta}\frac{\mathrm{d}^{\alpha+\gamma-\beta}\varepsilon(t)}{\mathrm{d}t^{\alpha+\gamma-\beta}}$	$P_f=\frac{C_\alpha}{C_\beta}\frac{\partial^{\alpha-\beta}}{\partial t^{\alpha-\beta}}$	$Q_f=C_\alpha\frac{\partial^\alpha}{\partial t^\alpha}+C_\gamma\frac{\partial^\gamma}{\partial t^\gamma}+\frac{C_\alpha C_\gamma}{C_\beta}\frac{\partial^{\alpha+\gamma-\beta}}{\partial t^{\alpha+\gamma-\beta}}$

Notes: $\alpha,\beta,\gamma\in(0,1)$, $\alpha-\beta>0$, and $\alpha+\gamma-\beta>0$.

2. General expression of viscoelastic models

In establishing a specific viscoelastic constitutive relationship, most scholars typically derive the relaxation compliance $G(t)$ or creep compliance $J(t)$ of a particular model. They then establish the stress-strain relationship by integrating the obtained $G(t)$ or $J(t)$ [39,43,44] according to the Boltzmann superposition principle, as shown in Eqs. (1) and (2), which are often labeled as 'hereditary' integrals because the value of $G(t)$ (or $J(t)$) depends on all previous history of $J(t)$ (or $G(t)$).

$$\sigma(t)=\varepsilon(0)G(t)+\int_0^t G(t-\tau)\dot{\varepsilon}(\tau)d\tau \quad \text{Eq. (1)}$$

$$\varepsilon(t)=\sigma(0)J(t)+\int_0^t J(t-\tau)\dot{\sigma}(\tau)d\tau \quad \text{Eq. (2)}$$

where $\sigma(t)$ and $\varepsilon(t)$ are time history stress and the corresponding strain, respectively. Performing a Laplace transform on the above equations, the relationship between relaxation and creep function in Laplace domain can be obtained ($\widehat{G}(s)\widehat{J}(s)=1/s^2$), which means that a single creep or relaxation test was able to determine all the relevant parameters in the viscoelastic model.

However, $G(t)/J(t)$ for different models varies, and for more complex models, $G(t)/J(t)$ can only be represented in the Laplace space but not explicitly in the time domain that manifests considerable challenges on both computation and application. In fact, all constitutive equations can be expressed as linear relationships between stress, strain, and their corresponding derivatives, as shown in Eq. (3).

$$f(\sigma,\dot{\sigma},\ddot{\sigma},\ldots,\varepsilon,\dot{\varepsilon},\ddot{\varepsilon},\ldots)=0 \quad \text{Eq.(3)}$$

Therefore, the general form of traditional viscoelastic constitutive models can be denoted as Eq. (4) [32].

$$P\sigma=Q\varepsilon \quad \text{Eq. (4)}$$

where P and Q are linear differential operators with respect to time, as shown in Eq. (5).

$$P=\sum_{r=0}^{a}p_r\frac{\partial^r}{\partial t^r},\ Q=\sum_{r=0}^{b}q_r\frac{\partial^r}{\partial t^r} \quad \text{Eq. (5)}$$

where $r\in\mathbb{N}$. For the FC constitutive model, it can still be signified as:

$$P_f\sigma=Q_f\varepsilon \quad \text{Eq. (6)}$$

In this case, P_f and Q_f are linear fractional differential operators, expressed in the same form as Eq. (5), but with $r\in\mathbb{R}^+$. It is important to note that when the FC model is employed to characterize the creep behavior of concrete, the derivative order r lies between (0, 1). This is because concrete occupies an intermediate state between an ideal solid and an ideal liquid, and in most cases, it is closer to an ideal solid, thus usually being nearer to 0. The formulas for P, Q, P_f, and Q_f in various commonly used models are detailed in Table 1.

The aforementioned constitutive equations are one-dimensional, where the detailed derivation for the expressions of fractional

constitutive formulas can be referred to literature [44]. Presently, these equations will be expanded to encompass three-dimensional constitutive relationships. Assuming directions of spherical stress and deviatoric stress are mutually independent, the spherical stress and deviatoric stress directions can be denoted as Eq. (7) and Eq. (8) respectively.

$$P'\sigma_{kk} = Q'\varepsilon_{kk} \quad \text{Eq. (7)}$$

$$P''S_{ij} = Q''e_{ij} \quad \text{Eq. (8)}$$

where σ_{kk} and ε_{kk} represent the spherical stress and strain (volumetric stress/strain), S_{ij} and e_{ij} denote the stress deviator and strain deviator, respectively. P' and Q' can be regarded as the differential operators P and Q in the one-dimensional constitutive expression, in which P'' and Q'' can be obtained through shear tests or derived from the constitutive equation by assuming a constant Poisson's ratio.

For isotropic materials, according to the Generalized Hooke's law, stress and strain can be decomposed into spherical stress/strain and deviatoric stress/strain components, respectively, as follows:

$$\sigma_{ij} = S_{ij} + \frac{1}{3}\sigma_{kk}\delta_{ij}, i, j = 1, 2, 3 \quad \text{Eq. (9)}$$

$$\varepsilon_{ij} = e_{ij} + \frac{1}{3}\varepsilon_{kk}\delta_{ij} \quad \text{Eq. (10)}$$

where δ_{ij} represents the Kronecker symbol, which equals 1 when $i = j$ and 0 when $i \neq j$. Substituting Eqs. (7) and (8) into Eq. (9) yields:

$$\sigma_{ij} = \frac{Q''}{P''}e_{ij} + \delta_{ij}\frac{1}{3}\frac{Q'}{P'}\varepsilon_{kk} \quad \text{Eq. (11)}$$

Substituting the modified Eq. (10) into Eq. (11) yields:

$$P''P'\sigma_{ij} = P'Q''\varepsilon_{ij} - \frac{1}{3}\delta_{ij}(P'Q'' - P''Q')\varepsilon_{kk} \quad \text{Eq. (12)}$$

Eq. (12) represents the three-dimensional tensor expression of any linear viscoelastic constitutive equation, where tensor subscripts follow the Einstein summation convention. The same derivation process applies to the FC viscoelastic constitutive, and its expression formula is:

$$P''_f P'_f \sigma_{ij} = P'_f Q''_f \varepsilon_{ij} - \frac{1}{3}\delta_{ij}\left(P'_f Q''_f - P''_f Q'_f\right)\varepsilon_{kk} \quad \text{Eq. (13)}$$

3. Discrete expression for viscoelastic materials

The preceding section established a general expression for the constitutive behavior of both traditional and fractional-order viscoelastic materials, followed by the derivation of three-dimensional viscoelastic material models assuming a constant Poisson's ratio. In this section, the implementation of these constitutive models will be demonstrated on the time scale through numerical solutions using finite differences and fractional calculus. The traditional Kelvin-Voigt viscoelastic model and an FC viscoelastic model will be used as examples in demonstrations.

3.1. Traditional model (Kelvin-Voigt model)

Taking the Kelvin-Voigt (KV) model as an example, which composed of a spring and a dashpot in parallel, as illustrated in Table 1, its constitutive equation is represented by Eq. (14).

$$\sigma(t) = k\varepsilon(t) + \eta\frac{\mathrm{d}\varepsilon(t)}{\mathrm{d}t} \quad \text{Eq. (14)}$$

In this model, $P = 1$ and $Q = k + \eta\frac{\partial}{\partial t}$. Assuming a constant Poisson's ratio (ν), this model is extended to three dimensions, as expressed in Eq. (12), and following formulations are given:

$$P' = P = 1; Q' = Q = k + \eta\frac{\partial}{\partial t}; P'' = P = 1; Q'' = \overline{Q} = \overline{k} + \overline{\eta}\frac{\partial}{\partial t} \quad \text{Eq. (15)}$$

where $\overline{k} = \frac{k}{2(1+\nu)}$ and $\overline{\eta} = \frac{\eta}{2(1+\nu)}$.

For concrete materials, the constant Poisson's ratio assumption is reasonable because variation in the Poisson's ratio is only applicable in scenarios where distinct time scales exist for the volumetric and deviatoric components. For the convenience of FE implementation, the spherical stress and deviatoric stress are calculated separately based on Eq. (12):

For $i = j = 1$:

$$P''P'\sigma_{xx} = P'Q''\varepsilon_{xx} - \frac{1}{3}(P'Q'' - P''Q')\varepsilon_v, \varepsilon_v = \varepsilon_{xx} + \varepsilon_{yy} + \varepsilon_{zz} \quad \text{Eq. (16)}$$

Substituting Eq. (15) into Eq. (16) yields:

$$\sigma_{xx} = \overline{k}\varepsilon_{xx} + \overline{\eta}\dot{\varepsilon}_{xx} - \frac{1}{3}(\overline{k} - k)\varepsilon_v - \frac{1}{3}(\overline{\eta} - \eta)\dot{\varepsilon}_v \quad \text{Eq. (17)}$$

For $i = j = 2$ or 3, the same expressions can be obtained for other two principal stress directions.
For $i \neq j$:

$$P''P'\sigma_{ij} = P'Q''\varepsilon_{ij} \quad \text{Eq. (18)}$$

Similarly, substituting the differential operators yields:

$$\sigma_{xy} = \overline{k}\varepsilon_{xy} + \overline{\eta}\dot{\varepsilon}_{xy} \quad \text{Eq. (19)}$$

Using a simple and stable backward difference method (FDM), one can obtain Eq. (20):

$$\dot{f}_{t+\Delta t} = \frac{\Delta f}{\Delta t};\ f_{t+\Delta t} = f_t + \Delta f \quad \text{Eq. (20)}$$

Substituting Eq. (20) into Eq. (17) and Eq. (19) and rearranging results, Eq. (21) and Eq. (22) are derived:

$$\Delta\sigma_{xx} = \left(\overline{k} + \frac{\overline{\eta}}{\Delta t}\right)\Delta\varepsilon_{xx} - \left(\frac{\Delta t(\overline{k} - k) + \overline{\eta} - \eta}{3\Delta t}\right)\Delta\varepsilon_v + \left(\overline{k}\varepsilon_{xx} - \frac{\overline{k} - k}{3}\varepsilon_v - \sigma_{xx}\right)_t \quad \text{Eq. (21)}$$

$$\Delta\sigma_{xy} = \left(\overline{k} + \frac{\overline{\eta}}{\Delta t}\right)\Delta\varepsilon_{xy} + (\overline{k}\varepsilon_{xx} - \sigma_{xx})_t \quad \text{Eq. (22)}$$

Eq. (21) and (22) represent the discretized expressions of stress, strain, and their increments over the time scale for the KV model.

3.2. FC viscoelastic model (single element)

According to Table 1, FC viscoelastic models can also be represented in the form of differential operators (P_f,Q_f). Taking a single FC model as an example, its constitutive equation is given by Eq. (23).

$$\sigma(t) = C_\beta D^\beta \varepsilon(t) \quad \text{Eq. (23)}$$

In this model, $P_f = 1, Q_f = C_\beta \frac{\partial^\beta}{\partial t^\beta}$. Likewise, assuming the constant Poisson's ratio (ν) during the loading process, the extension of this constitutive model to three dimensions yields the parameters as shown in Eq. (24), where the order of fractional differentiation (β) remains the same [32].

$$P'_f = 1;\ P''_f = 1;\ Q'_f = C_\beta \frac{\mathrm{d}^\beta}{\mathrm{d}t^\beta};\ Q''_f = \overline{C}_\beta \frac{\mathrm{d}^\beta}{\mathrm{d}t^\beta} \quad \text{Eq. (24)}$$

where $\overline{C}_\beta = \frac{C_\beta}{2(1+\nu)}$.

Substituting Eq. (24) into Eq. (13) gives:

$$\sigma_{ij} = \overline{C}_\beta D^\beta \varepsilon_{ij} - \frac{1}{3}\delta_{ij}(\overline{C}_\beta - C_\beta)D^\beta \varepsilon_{kk} \quad \text{Eq. (25)}$$

For $i = j = 1$:

$$\sigma_{xx} = \overline{C}_\beta D^\beta \varepsilon_{xx} - \frac{1}{3}(\overline{C}_\beta - C_\beta)D^\beta \varepsilon_v \quad \text{Eq. (26)}$$

For $i \neq j$:

$$\sigma_{xy} = \overline{C}_\beta D^\beta \varepsilon_{xy} \quad \text{Eq. (27)}$$

Evident challenges arise in the application of FDM (Eq. (20)) to Eqs. (26) and (27). Thus, a numerical integration method employing fractional derivatives is necessary. Although various methods have been proposed [45–48], these methods have different applicability conditions, primarily due to the varied definitions of fractional calculus.

In this study, the numerical approach proposed by Jin et al., in 2015 [49] for calculating Caputo-type fractional derivatives is employed. The advantage of this Caputo fractional derivative lies in its property that the derivative of a constant function is always zero, and its form is relatively concise, facilitating practical engineering applications.

For a derivative order β within the range (0,1), Eq. (28) provides a discretized representation of the β-order derivative of the function $f(t)$ based on the Caputo definition at uniformly spaced time intervals [49]:

$$\frac{\partial^\beta f(t_{n+1})}{\partial t^\beta} = \frac{1}{\Gamma(1-\beta)}\sum_{k=0}^{n}\int_{t_k}^{t_{k+1}} (t_{k+1} - s)^{-\beta}\frac{\partial f(s)}{\partial s}ds \quad \text{Eq. (28)}$$

$$= \frac{1}{\Gamma(1-\beta)}\sum_{k=0}^{n}\frac{f(t_{k+1}) - f(t_k)}{\Delta t}\int_{t_j}^{t_{j+1}} (t_{n+1} - s)^{-\beta}ds + r_{\beta,\Delta t}^{n+1}$$

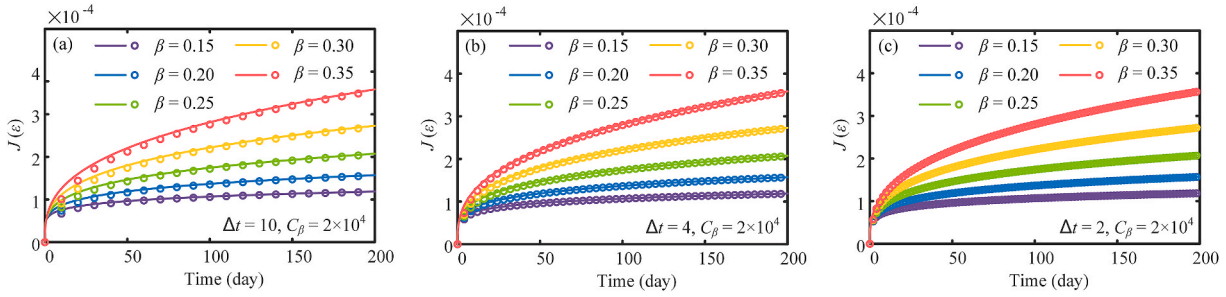

Fig. 1. Comparison between numerical and analytical solution.

Table 2
Comparison between numerical results and analytical solution with different parameters.

Err.	$\beta = 0.15$	$\beta = 0.20$	$\beta = 0.25$	$\beta = 0.30$	$\beta = 0.35$
$\Delta t = 10$	0.0382	0.0498	0.0608	0.0713	0.0813
$\Delta t = 4$	0.0193	0.0253	0.0310	0.0366	0.0419
$\Delta t = 2$	0.0112	0.0147	0.0181	0.0214	0.0245
$\Delta t = 1$	0.0064	0.0084	0.0103	0.0122	0.0141
$\Delta t = 0.1$	0.0009	0.0012	0.0015	0.0017	0.0020

$$= \frac{1}{\Gamma(2-\beta)} \sum_{k=0}^{n} d_{\beta,k} \frac{f(t_{n+1-k}) - f(t_{n-k})}{\Delta t^{\beta}} + r_{\beta,\Delta t}^{n+1}$$

where $d_{\beta,k} = (k+1)^{1-\beta} - k^{1-\beta}$, and $r_{\beta,\Delta t}^{n+1}$ represents the truncation error.

It can be observed from Eq. (28) that the most attractive aspect of using fractional operators in the viscoelastic constitutive laws is that the stress/strain response depends on the previous stress/strain history, which allows the long "fading" memory of the material to be taken into account.

In Eq. (28), when $j = 0$ and $d_{\beta,j} = 1, f(t_{n+1-j}) - f(t_{n-j}) = f(t_{n+1}) - f(t_n) = \Delta f(t_n)$. Therefore, Eq. (28) can be written as Eq. (29).

$$\frac{d^{\beta} f(t_{n+1})}{dt^{\beta}} = \frac{1}{\Delta t^{\beta} \Gamma(2-\beta)} \left(\Delta f(t_n) + \sum_{k=1}^{n} d_{\beta,k} (f(t_{n+1-k}) - f(t_{n-k})) \right) + r_{\beta,\Delta t}^{n+1} \quad \text{Eq. (29)}$$

Let $\sigma(t) = \delta(t)$ (unit step function), the strain response corresponding to Eq. (23) is the creep compliance of the material, and its analytical solution is given by:

$$J(t) = \frac{1}{C_{\beta} \Gamma(\beta+1)} t^{\beta} \quad \text{Eq. (30)}$$

Here, Γ represents the gamma function, as shown in Eq. (31).

$$\Gamma(\alpha) = \int_0^{\infty} e^{-t} t^{\alpha-1} dt \quad \text{Eq. (31)}$$

Substituting Eqs. (28) and (29) after discarding the truncation error into the constitutive Eq. (23) yields the approximate numerical solution for the creep behavior of the material:

$$\widehat{J}(t_{n+1}) - \widehat{J}(t_n) = \frac{\Delta t^{\beta} \Gamma(2-\beta)}{C_{\beta}} - \sum_{k=1}^{n} d_{\beta,k} (\widehat{J}(t_{n+1-k}) - \widehat{J}(t_{n-k})) \quad \text{Eq. (32)}$$

By recursion, the creep response at any given time can be obtained using Eq. (32). It's apparent that the accuracy of the numerical solution depends on the time interval Δt. Therefore, it is essential to compare the numerical solutions obtained with different time intervals to the theoretical solution given by Eq. (29). The comparison results are illustrated in Fig. 1. It is evident that the numerical results exhibit a favorable agreement with the theoretical solution.

The relative errors between the theoretical and numerical solutions are calculated using Eq. (33), (the symbol N denotes the number of calculated time nodes). The error trends for different time steps and various fractional derivative orders are summarized in Table 2, where errors are found to decreases as the time step reduces. Notably, with $\Delta t = 2$, the numerical results closely approximate the theoretical solution. Moreover, with an increase in the derivative order (β), the error tends to increase though acceptable limits remain.

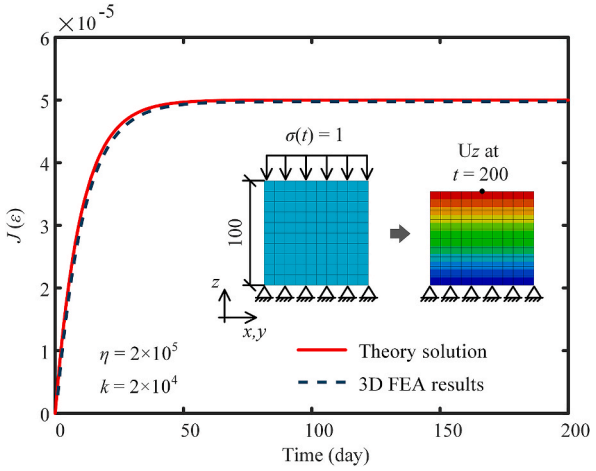

Fig. 2. Theoretical vs. FE analysis of KV model.

$$Err. = \frac{1}{N}\sum_{i=1}^{N}\frac{|J(i) - \widehat{J}(i)|}{J(i)} \quad \text{Eq. (33)}$$

4. Programming and validation of UMAT

FE simulations implementing the material constitutive relations were conducted based on the subroutine utilizing the UMAT interface provided by the commercial FE software ABAQUS, in which the UMAT subroutine can define arbitrary mechanical constitutive relations of materials. It is invoked at each iteration during the solution process at the integration points of the element, ensuring that the stress and strain of the material satisfy user-defined relationships. Therefore, in the UMAT subroutine, it is necessary to update the corresponding stress state and stress increment. Additionally, the corresponding Jacobian matrix has to be provided because the entire solution process is discretized into a series of steps in ABAQUS solver. The stress state at each step is determined by adding the stress increment from the previous step multiplied by the Jacobian matrix (Eq. (34)). For linear-elastic-small-deformation materials, the Jacobian matrix is equivalent to the stiffness matrix.

$$\boldsymbol{\sigma}^{t+\Delta t} = \boldsymbol{\sigma}^{t} + \mathrm{d}\boldsymbol{\sigma} = \boldsymbol{\sigma}^{t} + \boldsymbol{D}\mathrm{d}\boldsymbol{\varepsilon} \quad \text{Eq. (34)}$$

For a general small-deformation material, the Jacobian matrix $\boldsymbol{D} = \partial\Delta\boldsymbol{\sigma}/\partial\Delta\boldsymbol{\varepsilon}$, where $\Delta\boldsymbol{\sigma}$ is the stress increment matrix and $\Delta\boldsymbol{\varepsilon}$ is the strain increment matrix. In the case of isotropic materials, non-zero elements only appear in the upper-left 3 × 3 block and the main diagonal elements of the lower-right block. Therefore, when expanded, it can be represented as a 6 × 6 matrix:

$$\boldsymbol{D} = \frac{\partial\Delta\boldsymbol{\sigma}}{\partial\Delta\boldsymbol{\varepsilon}} = \begin{bmatrix} \frac{\partial\Delta\sigma_{11}}{\partial\Delta\varepsilon_{11}} & \frac{\partial\Delta\sigma_{11}}{\partial\Delta\varepsilon_{22}} & \frac{\partial\Delta\sigma_{11}}{\partial\Delta\varepsilon_{33}} & 0 & 0 & 0 \\ & \frac{\partial\Delta\sigma_{22}}{\partial\Delta\varepsilon_{22}} & \frac{\partial\Delta\sigma_{22}}{\partial\Delta\varepsilon_{33}} & 0 & 0 & 0 \\ & & \frac{\partial\Delta\sigma_{33}}{\partial\Delta\varepsilon_{33}} & 0 & 0 & 0 \\ & & & \frac{\partial\Delta\sigma_{12}}{\partial\Delta\varepsilon_{12}} & 0 & 0 \\ & Sym. & & & \frac{\partial\Delta\sigma_{13}}{\partial\Delta\varepsilon_{13}} & 0 \\ & & & & & \frac{\partial\Delta\sigma_{23}}{\partial\Delta\varepsilon_{23}} \end{bmatrix}. \quad \text{Eq. (35)}$$

4.1. Traditional model (Kelvin-Voigt model)

In the previous section, the three-dimensional constitutive model for the KV model was derived, as presented in Eqs. (21) and (22). To update the stress and stress increment within the UMAT subroutine, these two equations are considered as functions of the strain increment. Subsequently, the partial derivatives with respect to the strain increment provide the coefficients in the Jacobian matrix, as shown in Eqs. (36)–(38).

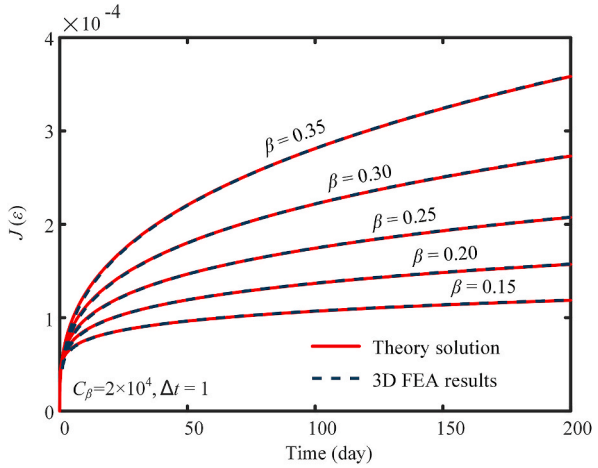

Fig. 3. Theoretical vs. FE analysis of FC model.

$$\frac{\partial \Delta\sigma_{xx}}{\partial \Delta\varepsilon_{xx}} = \left(\overline{k} + \frac{\overline{\eta}}{\Delta t}\right) - \left(\frac{\Delta t(\overline{k} - k) + \overline{\eta} - \eta}{3\Delta t}\right) \quad \text{Eq. (36)}$$

$$\frac{\partial \Delta\sigma_{xx}}{\partial \Delta\varepsilon_{yy}} = -\left(\frac{\Delta t(\overline{k} - k) + \overline{\eta} - \eta}{3\Delta t}\right) \quad \text{Eq. (37)}$$

$$\frac{\partial \Delta\sigma_{xy}}{\partial \Delta\varepsilon_{xy}} = \overline{k} + \frac{\overline{\eta}}{\Delta t} \quad \text{Eq. (38)}$$

In Eqs. (36)–(38), $k, \eta, \overline{k}$, and $\overline{\eta}$ are unknown variables that should be provided as input variables in the subroutine. For materials with a constant Poisson's ratio, only k, η, and υ need to be specified, while remaining variables are accessible within the UMAT subroutine.

To validate the subroutine, a standard cube with a side length of 100 mm is modeled. A constant unit axial pressure load is applied to the top surface, with a calculation time interval $\Delta t = 1$. The translational and rotational movements of the bottom surface are constrained. In Eq. (14), by setting $\sigma(t) = \delta(t)$ (unit step function), the creep theoretical solution of the KV model can be obtained:

$$J(t) = \frac{1}{k}\left(1 - \exp\left(-\frac{k}{\eta}t\right)\right) \quad \text{Eq. (39)}$$

Extracting the displacement of the top nodes from the FE model and converting it into strain for comparison with the theoretical solution (Fig. 2), it is evident that the FE results closely match the theoretical solution, demonstrating the reliability of the subroutine.

4.2. viscoelastic model

As for FC viscoelastic model, Eq. (32) is substituted into Eqs. (26) and (27) following identical approach, combined with the application of FDM, so one can yield Eqs. (40) and (41).

For $i = j = 1$:

$$\psi_\beta \Delta\sigma_{xx} = \overline{C}_\beta\left(\Delta\varepsilon_{xx} + \Theta^\beta_{exx}\right) - \frac{\left(\overline{C}_\beta - C_\beta\right)\left(\Delta\varepsilon_v + \Theta^\beta_{ev}\right)}{3} - \psi_\beta\sigma_{xx} \quad \text{Eq. (40)}$$

For $i \neq j$:

$$\psi_\beta \Delta\sigma_{xx} = \overline{C}_\beta\left(\Delta\varepsilon_{xy} + \Theta^\beta_{exy}\right) - \psi_\beta\sigma_{xy} \quad \text{Eq. (41)}$$

Similarly, performing partial differentiation on Equations (39) and (40) yields the coefficients in the Jacobian matrix:

$$\frac{\partial \Delta\sigma_{xx}}{\partial \Delta\varepsilon_{xx}} = \frac{\overline{C}_\beta}{\psi_\beta} - \frac{\overline{C}_\beta - C_\beta}{3\psi_\beta} \quad \text{Eq. (42)}$$

$$\frac{\partial \Delta\sigma_{xx}}{\partial \Delta\varepsilon_{yy}} = -\frac{\overline{C}_\beta - C_\beta}{3\psi_\beta} \quad \text{Eq. (43)}$$

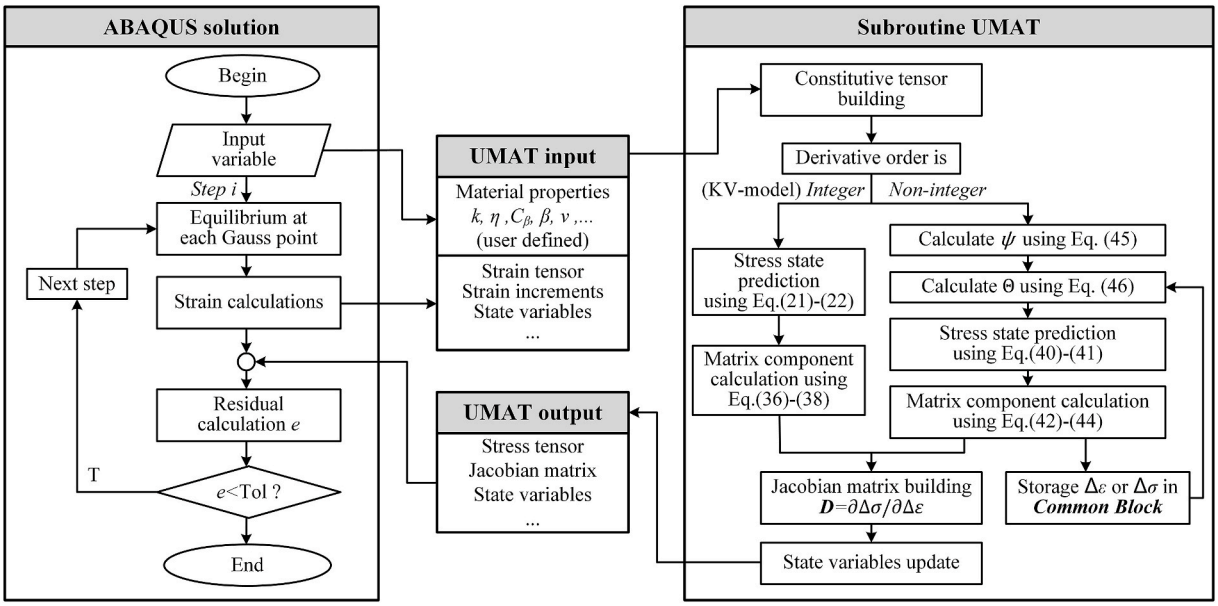

Fig. 4. The principles and flowchart of FE implementation.

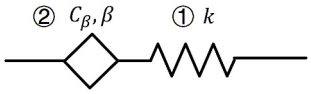

Fig. 5. Time-dependent constitutive model for concrete.

$$\frac{\partial \Delta\sigma_{xy}}{\partial \Delta\varepsilon_{xy}} = \frac{\overline{C}_\beta}{\psi_\beta} \quad \text{Eq. (44)}$$

In Eqs. (40)–(44):

$$\psi_\beta = \Delta t^\beta \cdot \Gamma(2-\beta) \quad \text{Eq. (45)}$$

$$\Theta^\beta_{\varepsilon ij} = \sum_{k=1}^{n} d_{\beta,k}\left(\varepsilon_{ij}(t_{n+1-k}) - \varepsilon_{ij}(t_{n-k})\right) \quad \text{Eq. (46)}$$

In the aforementioned equations, the unknown parameters are $\overline{C}_\beta, C_\beta$ and β, while the remaining variables can also be accessed throughout the calculation procedure. Notably, the FC model differs from conventional viscoelastic models that it requires the recording of strain history during the calculated process. In Abaqus subroutine, solution-dependent state variable (DEPVAR) can be employed as user-defined historical data at each Gauss integration point. However, this variable needs to be pre-defined before the calculation, and the upper limit for state variables is 1000, which might be insufficient for extended material creep analyses over prolonged durations. Consequently, this issue is addressed in this study by storing strain history in COMMON blocks (CB) developed by Refs. [37,38] Fortran. This storage space enables data transfer among program iterations by utilizing the stack memory of the computer system. Establishing a FE model and applying identical boundary conditions as shown in Fig. 2, the FE calculated results are compared with the analytical solution (Eq. (30)), as depicted in Fig. 3. It is shown that the FE strain closely aligns with the theoretical results for various orders (β).

Based on the derived and analyzed processes above, the FE implementation and principles of viscoelastic materials can be summarized in Fig. 4.

5. Time-dependent deformation model for concrete: case study

In the previous section, FE simulations of material deformation over time were exemplified by the traditional KV model and the single element FC model. In this section, a FC model specifically applicable to concrete is proposed. The derivation of its numerically discrete solution method on the time scale is also presented, as well as its implementation in FE simulations. The reliability of the model is validated through several case studies.

5.1. Development of 3D time-dependent constitutive relations for concrete

The time-dependent deformation of concrete consists of elastic, creep, shrinkage, and temperature deformation. Elastic and creep deformation are stress-dependent, while the latter two are stress-independent deformations. This paper aims to establish a constitutive relationship capable of describing the deformation behavior of concrete specimens under loading. Therefore, the consideration is currently limited to elastic and creep deformations, while shrinkage and temperature-induced deformations are beyond consideration.

As illustrated in Fig. 5, a FC viscoelastic model is proposed. This model comprises an elastic spring (①) and an FC element (②) connected in series, representing creep and elastic deformations of concrete, respectively.

In this model, the two basic elements jointly sustain the applied load. Consequently, the strain of the entire model is the sum of the strains of the two elements, whose stress is identical. This loading characteristic aligns with the additive nature that elastic and creep deformations in concrete can be calculated separately and then superimposed (Boltzmann superposition principle). Based on this characteristic, the constitutive equation for this model can be expressed as Eq. (47).

$$\sigma(t)+\frac{C_\beta}{k}\frac{\mathrm{d}^\beta\sigma(t)}{\mathrm{d}t^\beta}=C_\beta\frac{\mathrm{d}^\beta\varepsilon(t)}{\mathrm{d}t^\beta} \quad \text{Eq. (47)}$$

Extending to the three-dimensional constitutive relations, the following parameters can be derived:

$$P_f'=1+p_1\frac{\mathrm{d}^\beta}{\mathrm{d}t^\beta};\ P_f''=1+\overline{p}_1\frac{\mathrm{d}^\beta}{\mathrm{d}t^\beta};\ Q_f'=q_1\frac{\mathrm{d}^\beta}{\mathrm{d}t^\beta};\ Q_f''=\overline{q}_1\frac{\mathrm{d}^\beta}{\mathrm{d}t^\beta} \quad \text{Eq. (48)}$$

where $p_1=\frac{C_\beta}{k}$; $\overline{p}_1=\frac{\overline{C}_\beta}{\overline{k}}$; $q_1=C_\beta$; and $\overline{q}_1=\overline{C}_\beta$. In the case of a constant Poisson's ratio (ν), the parameters are given by: $\overline{C}_\beta=\frac{C_\beta}{2(1+\nu)}$, $\overline{k}=\frac{k}{2(1+\nu)}$. Substituting above items into Eq. (13) yields the three-dimensional expression of the constitutive relationship:

$$\sigma_{ij}+(p_1+\overline{p}_1)D^\beta\sigma_{ij}+p_1\overline{p}_1D^{2\beta}\sigma_{ij}=\overline{q}_1D^\beta\varepsilon_{ij}+p_1\overline{q}_1D^{2\beta}\varepsilon_{ij}-\frac{1}{3}\delta_{ij}\left[\varepsilon_{kk}+(p_1+\overline{p}_1-q_1)D^\beta\varepsilon_{kk}+(p_1\overline{p}_1-\overline{p}_1q_1)D^{2\beta}\varepsilon_{kk}\right] \quad \text{Eq. (49)}$$

For $i=j=1$:

$$\sigma_{xx}+(p_1+\overline{p}_1)D^\beta\sigma_{xx}+p_1\overline{p}_1D^{2\beta}\sigma_{xx}=\overline{q}_1D^\beta\varepsilon_{xx}+p_1\overline{q}_1D^{2\beta}\varepsilon_{xx}-\frac{1}{3}\left[\varepsilon_v+(p_1+\overline{p}_1-q_1)D^\beta\varepsilon_v+(p_1\overline{p}_1-\overline{p}_1q_1)D^{2\beta}\varepsilon_v\right] \quad \text{Eq. (50)}$$

For $i\neq j$:

$$\sigma_{xy}+(p_1+\overline{p}_1)D^\beta\sigma_{xy}+p_1\overline{p}_1D^{2\beta}\sigma_{xy}=\overline{q}_1D^\beta\varepsilon_{xy}+p_1\overline{q}_1D^{2\beta}\varepsilon_{xy} \quad \text{Eq. (51)}$$

Likewise, substituting Eq. (32) into Eqs. (50) and (51), and combining with FDM, the stress-strain relationship is expressed in terms of states and increments:

For $i=\text{Eq.}\,j=1$:

$$\begin{aligned}&\psi_\beta\psi_{2\beta}\sigma_{xx}+\left[\psi_\beta\psi_{2\beta}+\psi_{2\beta}(p_1+\overline{p}_1)+\psi_\beta p_1\overline{p}_1\right]\Delta\sigma_{xx}+\psi_{2\beta}(p_1+\overline{p}_1)\Theta_{\sigma xx}^\beta+\psi_\beta p_1\overline{p}_1\Theta_{\sigma xx}^{2\beta}=\overline{q}_1\psi_{2\beta}\left(\Delta\varepsilon_{xx}+\Theta_{\varepsilon xx}^\beta\right)+p_1\overline{q}_1\psi_\beta\left(\Delta\varepsilon_{xx}+\Theta_{\sigma xx}^{2\beta}\right)\\&-\frac{1}{3}\left\{\psi_\beta\psi_{2\beta}\varepsilon_v+\psi_{2\beta}(p_1+\overline{p}_1-q_1)\left(\Delta\varepsilon_v+\Theta_{\varepsilon v}^\beta\right)+\psi_\beta(p_1\overline{p}_1-\overline{p}_1q_1)\left(\Delta\varepsilon_v+\Theta_{\varepsilon v}^{2\beta}\right)\right\}\end{aligned} \quad \text{Eq. (52)}$$

For $i\neq j$:

$$\psi_\beta\psi_{2\beta}\sigma_{xy}+\left[\psi_\beta\psi_{2\beta}+\psi_{2\beta}(p_1+\overline{p}_1)+\psi_\beta p_1\overline{p}_1\right]\Delta\sigma_{xy}+\psi_{2\beta}(p_1+\overline{p}_1)\Theta_{\sigma xy}^\beta+\psi_\beta p_1\overline{p}_1\Theta_{\sigma xy}^{2\beta}=\overline{q}_1\psi_{2\beta}\left(\Delta\varepsilon_{xy}+\Theta_{\varepsilon xy}^\beta\right)+p_1\overline{q}_1\psi_\beta\left(\Delta\varepsilon_{xy}+\Theta_{\sigma xy}^{2\beta}\right) \quad \text{Eq. (53)}$$

Coefficients in the Jacobian matrix can be calculated as follows:

$$\frac{\partial\Delta\sigma_{xx}}{\partial\Delta\varepsilon_{xx}}=\frac{\overline{q}_1\psi_{2\beta}+p_1\overline{q}_1\psi_\beta}{\psi_\beta\psi_{2\beta}+\psi_{2\beta}(p_1+\overline{p}_1)+\psi_\beta p_1\overline{p}_1}-\frac{\psi_{2\beta}(p_1+\overline{p}_1-q_1)+\psi_\beta(p_1\overline{p}_1-\overline{p}_1q_1)}{3\left[\psi_\beta\psi_{2\beta}+\psi_{2\beta}(p_1+\overline{p}_1)+\psi_\beta p_1\overline{p}_1\right]} \quad \text{Eq. (54)}$$

$$\frac{\partial\Delta\sigma_{xx}}{\partial\Delta\varepsilon_{yy}}=-\frac{\psi_{2\beta}(p_1+\overline{p}_1-q_1)+\psi_\beta(p_1\overline{p}_1-\overline{p}_1q_1)}{3\left[\psi_\beta\psi_{2\beta}+\psi_{2\beta}(p_1+\overline{p}_1)+\psi_\beta p_1\overline{p}_1\right]} \quad \text{Eq. (55)}$$

$$\frac{\partial\Delta\sigma_{xy}}{\partial\Delta\varepsilon_{xy}}=\frac{\overline{q}_1\psi_{2\beta}+p_1\overline{q}_1\psi_\beta}{\psi_\beta\psi_{2\beta}+\psi_{2\beta}(p_1+\overline{p}_1)+\psi_\beta p_1\overline{p}_1} \quad \text{Eq. (56)}$$

In Eqs. (52)–(56), ψ and Θ can be calculated using Eqs. (44) and (45). Thus, it is only necessary to input the corresponding parameters for the material $(p_1,\overline{p}_1,q_1,\overline{q}_1)$ into the UMAT program.

5.2. Case study—Creep experiment on reinforced concrete

Existing creep experiments mainly focus on plain concrete subjected to axial loads, in which the creep response is primarily

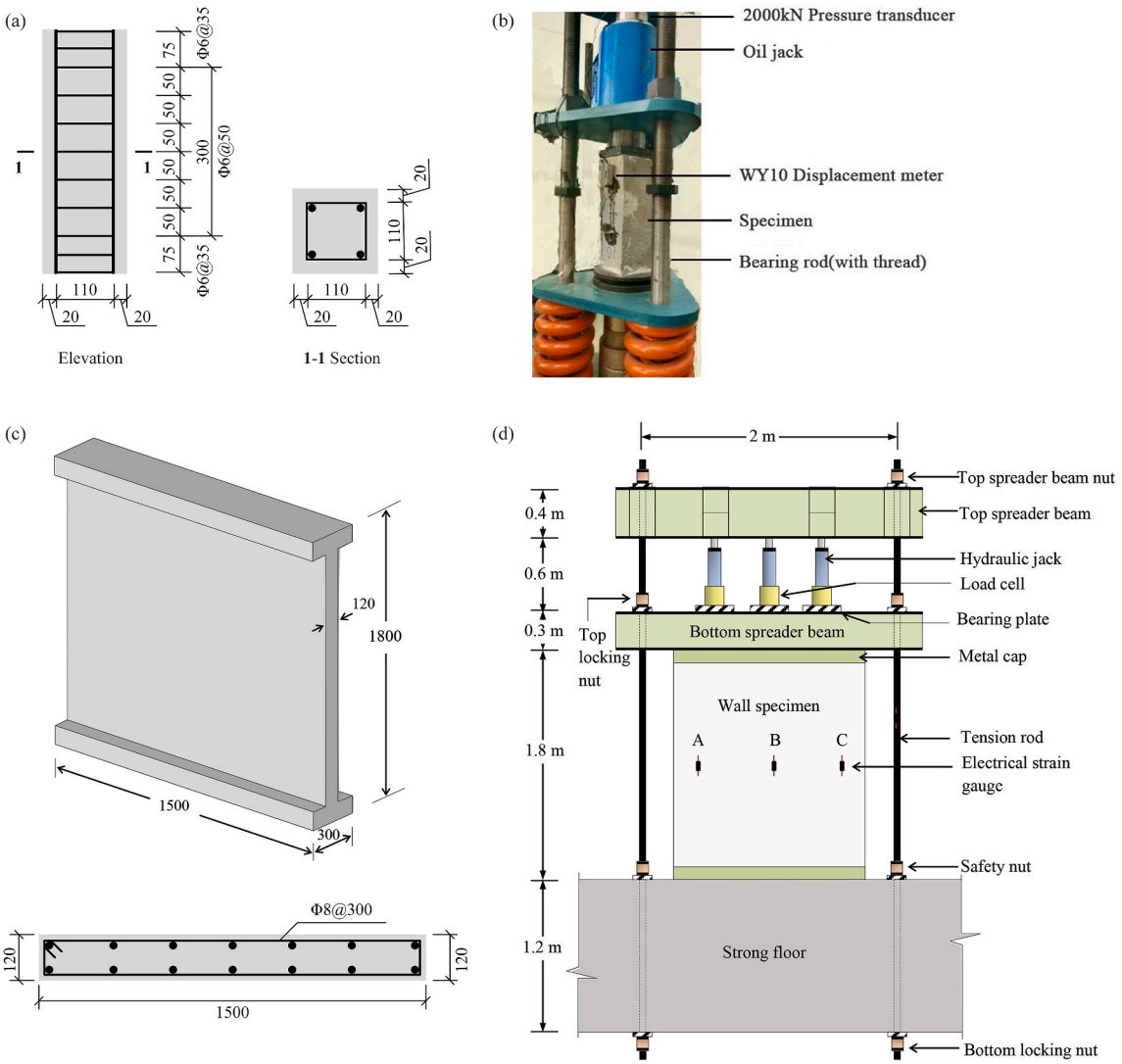

Fig. 6. Detailed information and loading arrangements of specimens: (a) Dimensions and reinforcement details of the specimen in Ref. [51]; (b) Loading setup for the specimen in Ref. [50]; (c) Dimensions and reinforcement details of the specimen in Ref. [50]; (d) Loading setup for the specimen in Ref. [50].

Table 3
Details information of the specimens.

ID of specimens	ρ_s, %	f_c, MPa	σ, MPa	t_0, Days
C30-0.28–1.40 %	1.40	35.0	12.33	62
C30-0.28–2.01 %	2.01			
C50-0.28–1.40 %	1.40	40.4	13.82	
C50-0.28–2.01 %	2.01			
C60-0.30–1.40 %	1.40	58.2	20.10	
C60-0.30–2.01 %	2.01			
W-NS-LR	0.39	51.7	4	8
W-NS-HR	2.43			

Notes: ρ_s, f_c, σ, and t_0 represent sectional reinforcement ratio, concrete strength, axial stress, and loading age, respectively. And the strain values from the references have been converted to strain responses under unit stress ((t)).

influenced by the internal composition of the concrete material. Therefore, FE results closely align with theoretical model solutions, as illustrated in Figs. 2 and 3. Consequently, when FE are employed to simulate creep, the emphasis lies in ensuring the accuracy of model parameters that can be optimized and regressively analyzed through experimental results. This study validates the FE model with two

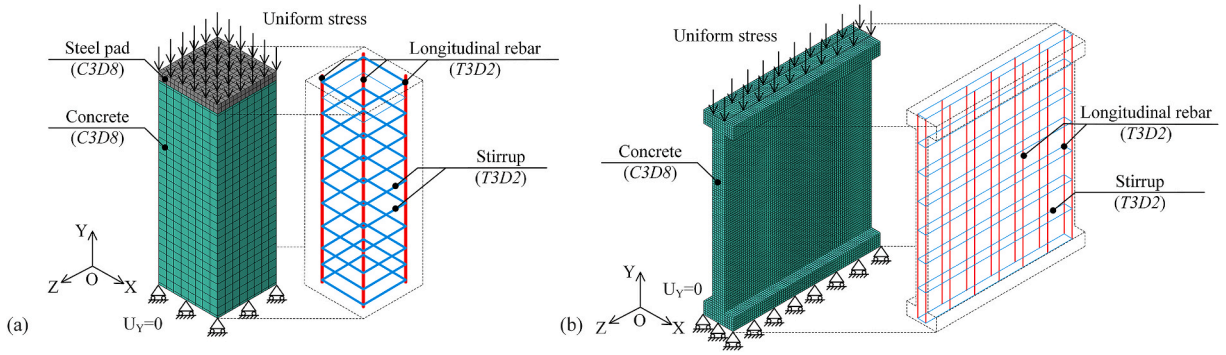

Fig. 7. FE model information and loading boundary conditions.

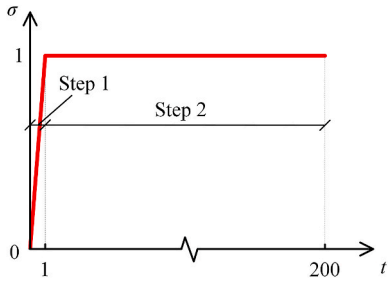

Fig. 8. Configuration of analysis steps.

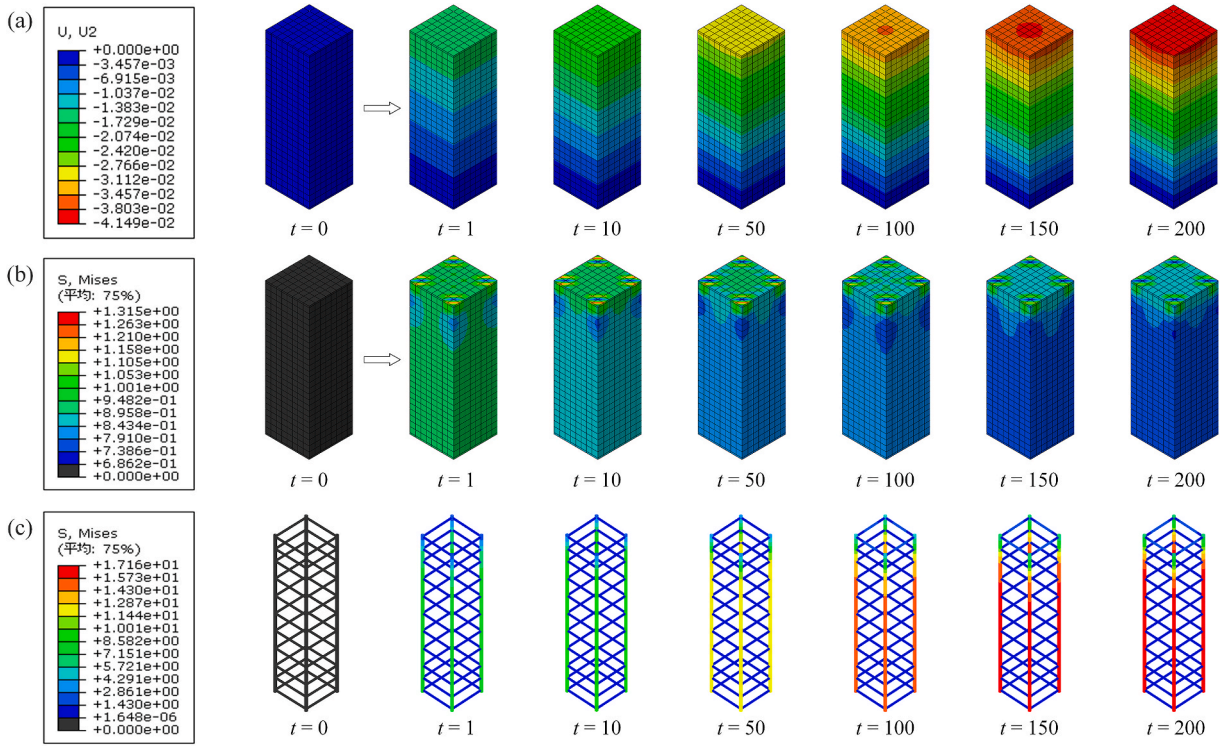

Fig. 9. FE results (C30-0.28–1.40 % [51]): (a) The relationship between axial displacement and time; (b) Concrete stress; (c) Reinforcement stress.

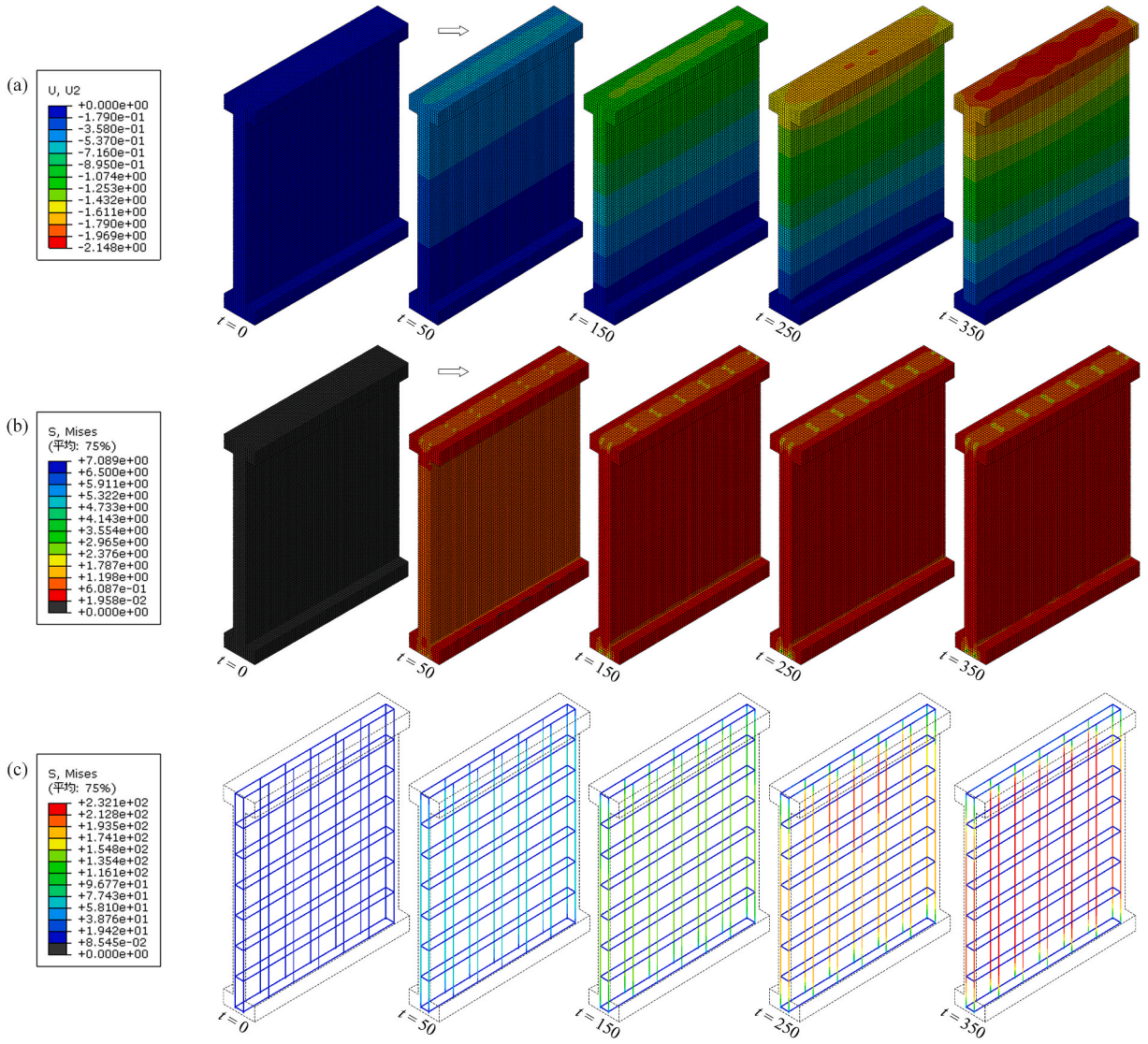

Fig. 10. FE results (W-NS-LR [49]): (a) The relationship between axial displacement and time; (b) Concrete stress; (c) Reinforcement stress.

sets of creep experiments on reinforced concrete [50,51]. One set comprises standard creep tests on 150 mm × 150 mm × 450 mm prismatic specimens conducted by a standard creep test apparatus. The other set involves creep tests on 1500 mm × 120 mm × 1800 mm shear walls, loaded using a reaction frame and hydraulic jacks. Each experimental set includes specimens with different longitudinal reinforcement ratios for comparative analysis. The reinforcement configurations and loading conditions are illustrated in Fig. 6, and specific details of each specimen are provided in Table 3.

The FE models of the specimens and their loading boundary conditions are depicted in Fig. 7. *C3D8* elements are employed for concrete, and *T3D2* truss elements are used for the reinforcement, respectively. The individual mesh size for hexahedral elements is selected as having a length of 20 mm. The constitutive relationship for concrete material is defined through UMAT, while a bi-linear model is adopted for the reinforcement material. The coupling between steel and concrete is achieved through embedment (as the creep experiments were conducted under stress levels significantly lower than the concrete strength, the bond slip between steel and concrete could be neglected). Due to the limitation in defining instantaneous loads during the static general analysis step in ABAQUS, a two-step analysis strategy is employed. In the initial step, time is set to 1, and a linear load ramp from 0 to 1 is established. Subsequently, in the second step, the load is held constant for a duration equal to the number of days corresponding to the experimental duration, as illustrated in Fig. 8.

The FE results for the first specimen in the first and second experimental set are presented in Figs. 9 and 10, respectively. It is apparent that the axial displacement of the specimens (Fig. 9(a)–. 10(a)) progressively increases with time, while the rate of change decreases as time elapses. The stress in concrete (Fig. 9(b)–. 10(b)) initially reaches its maximum upon loading and gradually decreases over time, while the stress in reinforcement exhibits an increasing trend (Figs. 9(c) and Fig. 10(c)). This observation indicates that,

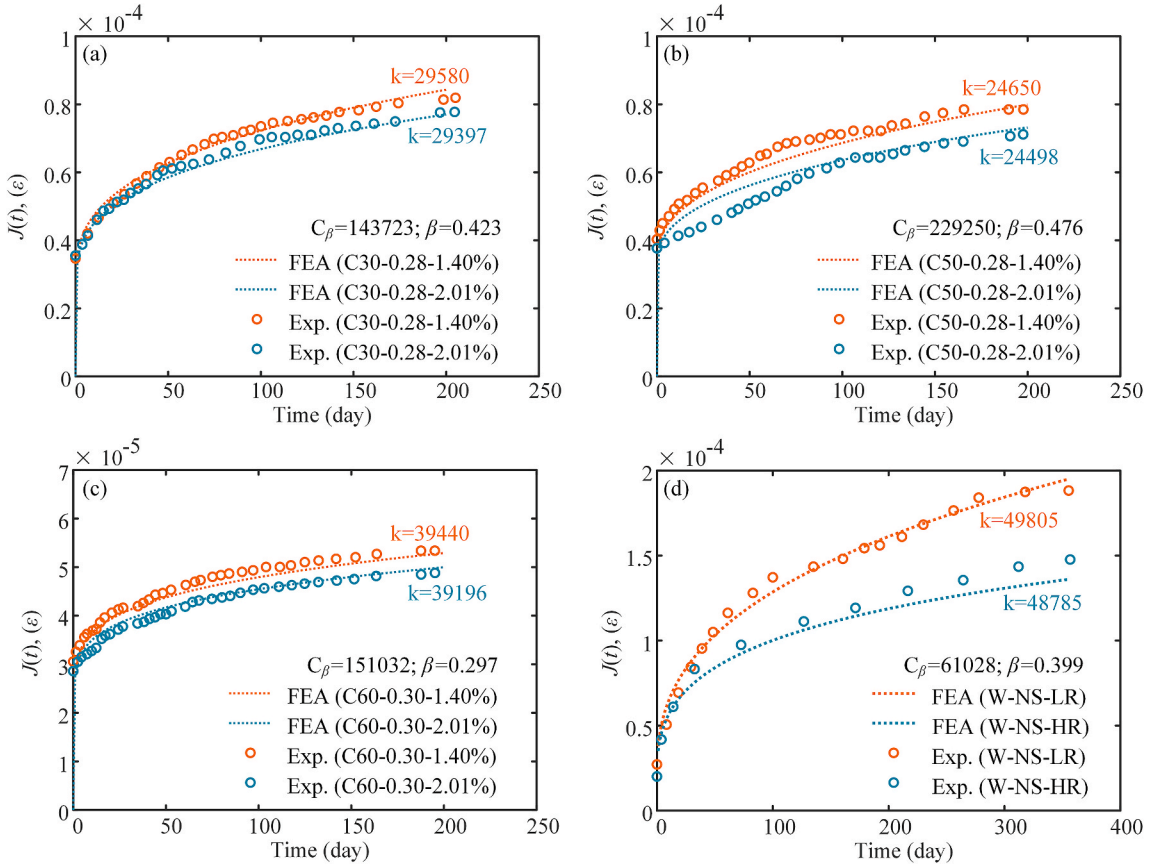

Fig. 11. Comparison of FE results and experimental strain.

under constant loading, the creep of concrete leads to a gradual transfer of stress from concrete to steel, aligning with the conclusions drawn in literature [3].

In experiments, vertical displacement was recorded at the upper and lower endpoints of the experimental strain measurement area. The experimental strain values were calculated by dividing the difference in displacement between these two points. The FE strain values were compared with the experimental strain results, as illustrated in Fig. 11. It can be observed that the FE results closely approximate the experimental results, demonstrating consistency in the deformation patterns of concrete strain over time.

6. Conclusions

This study proposes an effective and widely applicable numerical method for traditional and fractional-order calculus viscoelastic models to simulate the time-dependent behavior of materials under loading. Exploiting the deformation characteristics of concrete, a theoretical model suitable for simulating the time-dependent deformation of concrete is also developed. Based on the expression of constitutive relations under the general definition of viscoelastic materials, this method enables the derivation and solution of numerical methods for viscoelastic models with arbitrary complexity. In summary, the following conclusions can be drawn.

(1) When simulating material deformation, highly complex constitutive forms are often required in conventional viscoelastic models, in which specific solution and parameter fitting processes are intricate, and the physical significance is unclear. Therefore, this study proposes a viscoelastic model based on fractional-order calculus to simulate the time-dependent behavior of materials. This model reduces the number of required parameters with enhanced fitting capabilities, while clear physical significances are maintained.

(2) The constitutive relations of both traditional and fractional-order calculus models are discretized in a unified expression on the time scale. For numerical solution methods, the fractional-order calculus models are solved using the numerical approach based on the Caputo-type defined integration. The influence of time interval on the solution accuracy is duly analyzed.

(3) By decomposing the stress and strain in the constitutive model into spherical and deviatoric components, the three-dimensional tensor constitutive expression for the model is obtained that allows its application in the three-dimensional domain. Then the model is implemented in commercial FE software, demonstrating its application value in engineering fields.

(4) Based on the deformation characteristics of concrete under loading, a concrete constitutive model using fractional-order derivatives is proposed. This model utilizes two basic elements to represent the elastic and creep deformations of concrete,

characterized by strong interpretability, clear physical significance, and fewer parameter inputs. Additionally, it demonstrates favorable fitting capabilities indicated by high consistency between FE and experimental results.

This method can be readily extended to any type of concrete, and even other materials, requiring only the recalibration of the parameters within the constitutive model. In future research, factors such as concrete aging time, environmental humidity, and environmental temperature can be incorporated into this model to achieve a comprehensive understanding of the stress-strain response of specimens under continuous multi-stage loading conditions in complex environments.

CRediT authorship contribution statement

Xianming Luo: Writing – original draft, Methodology, Investigation, Formal analysis, Data curation, Conceptualization. **Yun Zhou:** Writing – review & editing, Supervision, Methodology, Funding acquisition, Formal analysis. **Fan Yi:** Writing – review & editing, Visualization, Validation, Data curation. **Weijian Yi:** Writing – review & editing, Visualization, Supervision, Conceptualization.

Declaration of competing interest

The authors declare that they have no conflict of interest.

Data availability

Data will be made available on request.

Acknowledgements

The authors sincerely appreciate the funding support provided by the National Natural Science Foundation of China (NSFC) (No. 51878264, No. 52278306), the Department of Science of Technology of Hunan Province (No. 2022SK2096), the Natural Science Foundation of Hunan Province of China (No. 2023JJ70003) and the Hydraulic Science of Technology Project of the Hunan Provincial Department of Water Resources (No. XSKJ2023059-31).

References

[1] A. De Sortis, P. Paoliani, Statistical analysis and structural identification in concrete dam monitoring, Eng. Struct. 29 (1) (2007) 110–120.
[2] L.B. Pan, P.C. Liu, S.L. Bakoss, Long-term shortening of concrete columns in tall buildings, J. Struct. Eng. 119 (7) (1992) 2258–2262.
[3] W.F. Baker, D.S. Korista, L.C. Novak, et al., Creep and shrinkage and the design of supertall buildings—a case study: the Burj Dubai Tower, ACI Journal SP 246–8 (2007) 133–148.
[4] F. Tahmasebinia, D. Fogerty, L.O. Wu, et al., Numerical analysis of the creep and shrinkage experienced in the Sydney Opera House and the rise of digital twin as future monitoring technology, Buildings 137 (9) (2019).
[5] S. Tiwari, G. Mondal, S.R. Dash, et al., Experimental investigation of unbonded reinforced concrete PT shear wall under lateral loading: a state-of-the-art review, J. Build. Eng. 78 (2023) 107504.
[6] ACI Committee 209, Prediction of Creep, Shrinkage, and Temperature Effects in Concrete Structures (209R-92), American Concrete Institute, 1992.
[7] CEB-FIP, Fib Model code for concrete structures 2010, International Federation for Structural Concrete (fib) (2010).
[8] Z.P. Bažant, L. Panula, Practical prediction of time-dependent deformations of concrete, Mater. Struct. 12 (69) (1978) 169–183.
[9] Z.P. Bažant, J.K. Kim, L. Panula, Improved prediction model for time-dependent deformations of concrete: Part 1-Shrinkage, Mater. Struct. 24 (1991) 327–345.
[10] Z.P. Bažant, J.K. Kim, Improved prediction model for time-dependent deformations of concrete: Part 2-Basic creep, Mater. Struct. 24 (1991) 409–421.
[11] Z.P. Bažant, W.P. Murphy, Creep and shrinkage prediction model for analysis and design of concrete structures-model B3, Mater. Struct. 28 (1995) 357–365.
[12] R. Wendner, M.H. Hubler, Z.P. Bažant, The B4 Model for multi-decade creep and shrinkage prediction, in: Ninth International Conference on Creep, Shrinkage, and Durability Mechanics (CONCREEP-9), 2013. MA, USA.
[13] N.J. Gardner, M.J. Lockman, Design provisions for drying shrinkage and creep of normal strength concrete, ACI Mater. J. 98 (2) (2001) 159–167.
[14] L.R. Laila, B.G.A. Gurupatham, K. Roy, et al., Influence of super absorbent polymer on mechanical, rheological, durability, and microstructural properties of self-compacting concrete using non-biodegradable granite pulver, Struct. Concr. 22 (2021) E1093–E1116.
[15] C.S. Madan, S. Munuswamy, P.S. Joanna, et al., Comparison of the flexural behavior of high-volume fly AshBased concrete slab reinforced with GFRP bars and steel bars, Journal of Composites Science 6 (6) (2022) 157.
[16] I. Carol, Z.P. Bažant, Viscoelasticity with aging caused by solidification of nonaging constituent, J. Eng. Mech. 119 (11) (1993) 2252–2269.
[17] S. Sathikumar, B.L. Karihaloo, S.G. Reid, A model for ageing visco-elastic tension softening materials, Mech. Cohesive-Frict. Mater. 3 (1) (1998) 27–39.
[18] B. Han, H. Xie, Z. Li, et al., Nonlinear model for early age creep of concrete under compression strains, Construct. Build. Mater. 147 (2017) 203–211.
[19] G.D. Luzio, Numerical model for time-dependent fracturing of concrete, J. Eng. Mech. 135 (7) (2009) 632–640.
[20] T. Honorio, B. Bary, F. Benboudjema, et al., Multiscale estimation of ageing viscoelastic properties of cement-based materials: a combined analytical and numerical approach to estimate the behaviour at early age, Cement Concr. Res. 85 (2016) 137–155.
[21] Z.P. Bažant, L. Cedolin, W.F. Chen, et al., Stability of structures: elastic, inelastic, fracture and damage theories, J. Struct. Eng. 119 (3) (1993) 1001–1002.
[22] A. Gemant, A method of analyzing experimental results obtained from elasto-viscous bodies, Physics 7 (8) (1936) 311–317.
[23] R. Ma, M. Ni, Q. Chen, et al., Viscoelastic fractional model based on harmonic excitation, Math. Probl Eng. 2022 (2022) 4799387.
[24] M.D. Paola, A. Pirrotta, A. Valenza, Visco-elastic behavior through fractional calculus: an easier method for best fitting experimental results, Mech. Mater. 43 (12) (2011) 799–806.
[25] A. Bonfanti, J.L. Kaplan, G. Charras, et al., Fractional viscoelastic models for power-law materials, Soft Matter 16 (26) (2020) 6002–6020.
[26] Y.A. Rossikhin, M.V. Shitikova, et al. Applications of fractional calculus to dynamic problems of linear and nonlinear hereditary mechanics of solids. Appl. Mech. Rev. 50(1): 16-67.
[27] Y. Bouras, Z. Vrcelj, Fractional and fractal derivative-based creep models for concrete under constant and time-varying loading, Construct. Build. Mater. 367 (2023) 130324.
[28] M.D. Paola, M.F. Granata, Fractional model of concrete hereditary viscoelastic behaviour, Arch. Appl. Mech. 87 (2) (2016) 335–348.
[29] H. Xu, X. Jiang, Creep constitutive models for viscoelastic materials based on fractional derivatives, Comput. Math. Appl. 73 (2017) 1377–1384.
[30] S. Paunović, M. Cajić, D. Karličić, et al., A novel approach for vibration analysis of fractional viscoelastic beams with attached masses and base excitation, J. Sound Vib. 463 (2019) 114955.

[31] J. Xu, Y. Chen, Y. Tai, et al., Vibration analysis of complex fractional viscoelastic beam structures by the wave method, Int. J. Mech. Sci. 167 (2020) 105204.
[32] N. Makris, Three-dimensional constitutive viscoelastic laws with fractional order time derivatives. Journal of Rheology, J. Rheol. 41 (5) (1997) 1007–1020.
[33] M. Oeser, S. Freitag, Fractional derivatives and recurrent neural networks in rheological modelling–part I: theory, Int. J. Pavement Eng. 17 (2) (2016) 87–102.
[34] M.D. Paola, M. Zingales, Exact mechanical models of fractional hereditary materials, J. Rheol. 56 (5) (2012) 983–1004.
[35] M.D. Paola, F.P. Pinnola, M.Z. Zingales, A discrete mechanical model of fractional hereditary materials, Meccanica 48 (7) (2013) 1573–1586.
[36] M. Enelund, L. Mähler, K. Runesson, et al., Formulation and integration of the standard linear viscoelastic solid with fractional order rate laws, Int. J. Solid Struct. 36 (16) (1999) 2417–2442.
[37] L. Gu, W. Zhang, T. Ma, et al., Numerical simulation of viscoelastic behavior of asphalt mixture using fractional constitutive model, J. Eng. Mech. 147 (5) (2021) 04021027.
[38] W. Quan, K. Zhao, X. Ma, et al., Fractional viscoelastic models for asphalt concrete: from parameter identification to pavement mechanics analysis, J. Eng. Mech. 148 (8) (2022) 04022036, 1.
[39] G. Alotta, O. Barrera, A. Cocks, et al., The finite element implementation of 3D fractional viscoelastic constitutive models, Finite Elem. Anal. Des. 146 (2018) 28–41.
[40] S. Liang, R. Luo, W. Luo, Fractional differential constitutive model for linear viscoelasticity of asphalt and asphalt mastic, Construct. Build. Mater. 306 (2021) 124886.
[41] L. Ma, F. Wang, P. Cui, et al., Effect of aging on the constitutive models of asphalt and their mixtures, Construct. Build. Mater. 272 (2021) 121611.
[42] G. Alotta, O. Barrera, A. Cocks, et al., On the behavior of a three-dimensional fractional viscoelastic constitutive model, Meccanica 52 (9) (2016) 2127–2142.
[43] A. Carini, P. Gelfi, E. Marchina, An energetic formulation for the linear viscoelastic problem. Part I: theoretical results and first calculations, Int. J. Numer. Methods Eng. 38 (1) (1995) 37–62.
[44] W. Chen, H. Sun, X. Li, Fractional Derivative Modeling in Mechanics and Engineering, Springer & Science Press Beijing, Singapore, 2022.
[45] M.M. Meerschaert, C. Tadjeran, Finite difference approximations for two-sided space-fractional partial differential equations, Appl. Numer. Math. 56 (1) (2006) 80–90.
[46] H. Jiang, F. Liu, I. Turner, et al., Analytical solutions for the multi-term time–space Caputo–Riesz fractional advection–diffusion equations on a finite domain, J. Math. Anal. Appl. 389 (2) (2012) 1117–1127.
[47] M. Gülsu, Y. Öztürk, A. Anapalı, Numerical approach for solving fractional relaxation–oscillation equation, Appl. Math. Model. 37 (8) (2013) 5927–5937.
[48] W. Bu, Y. Tang, J. Yang, Galerkin finite element method for two-dimensional Riesz space fractional diffusion equations, J. Comput. Phys. 276 (2014) 26–38.
[49] B. Jin, R. Lazarov, Y. Liu, et al., The Galerkin finite element method for a multi-term time-fractional diffusion equation, J. Comput. Phys. 281 (2015) 825–843.
[50] M.N. Shariff, M. Devdas, Experimental studies on creep and shrinkage behavior of reinforced concrete walls, ACI Struct. J. 117 (3) (2020) 249–260.
[51] P. Chen, G. Zhang, S. Cao, et al., Creep and post-creep mechanical properties of reinforced concrete columns, J. Build. Eng. 63 (2023) 105521.